

# Technical performance of the HEGRA IACT system

G. Pühlhofer, A. Kohnle, and O. Bolz, for the HEGRA collaboration

Max-Planck-Institut für Kernphysik, Postfach 103980, D-69029 Heidelberg, Germany

**Abstract.** Since the beginning of 1997, the HEGRA collaboration is running a stereoscopic system of 4 (later 5) imaging atmospheric Cherenkov telescopes on the Canary Island La Palma. In this paper we show the basic calibration schemes which were developed for the system and some results. Key features are the continuous sensitivity monitoring with an accuracy of a few percent, the absolute pointing accuracy of 25 arcsec, and an absolute energy calibration with an accuracy of 15 percent. The sensitivity monitoring has shown that the energy threshold of the system with a nominal value of 500 GeV (at low zenith angles) has not exceeded 600 GeV throughout the whole operation time.

---

## 1 Introduction

The HEGRA Stereoscopic Imaging Atmospheric Cherenkov Telescope (IACT) System is located on the Roque de los Muchachos on the Canary Island La Palma, at 2200 m above sea level. It consists of 5 identical telescopes (CT 2 - CT 6), which operate in coincidence for the stereoscopic detection of air showers induced by primary  $\gamma$ -rays in the atmosphere, using the Cherenkov light emitted by the shower particles. There is also a single telescope (CT 1) running in stand-alone mode which is not discussed in this paper.

The first four system telescopes (CT 3 - CT 6) were installed during 1995 and 1996. The system has been running in a stable configuration since March 1997; major changes were the reduction of the pixel threshold to the final value of 6 photoelectrons (ph.e.) in May 1997, and the upgrade of the CT 2 electronics and its inclusion into the system in August 1998. The hardware and the performance as well as the Monte Carlo simulations are described in Daum et al. (1997) and Konopelko et al. (1999). Table 1 gives an overview of the system detector parameters.

In this paper we will mainly concentrate on the long-term

---

Correspondence to: G. Pühlhofer  
(Gerd.Puehlhofer@mpi-hd.mpg.de)

calibration and stability of the telescopes throughout several years of operation. The calibration of the system telescopes comprises the following major issues: • geometric calibration, • continuous camera electronics calibration, • relative sensitivity monitoring, and • absolute energy threshold, which will be covered in the following sections.

## 2 Geometric calibration

### 2.1 Telescope pointing

The pointing of the system telescopes is corrected using an analytical model of the telescopes' mechanical structure. This model allows to compute the mispointing for any given telescope elevation and azimuth angle. The same model works for all system telescopes, but of course different model parameters apply for each of the five telescopes. The calibration procedure makes use of observing a sample of stars as reference sources with the telescopes, by performing so-called *point runs*. The initial pointing calibration was completed during the telescopes' commissioning phase. Afterwards, the model parameters needed to be redetermined only on special occasions, such as a telescope mirror readjustment or a dis- and remounting of the shaft encoders. The remaining systematic pointing error is about 25'' in right ascension and declination. This value was derived from the calibration itself. The calibration procedure is described in more detail in Pühlhofer et al. (1997).

The temporal stability and accuracy of the pointing calibration throughout the entire operation time of the telescope system is demonstrated here by the examination of the center of gravity of the TeV emission of the Crab Nebula. Figure 1 shows the sky region around the Crab Nebula in celestial coordinates. As reference, the Chandra X-ray image is shown in the background. The apparent position of the Crab pulsar, being in the center of the X-ray image, was placed in Fig. 1 at the year 2000-coordinates of the pulsar, as measured in the radio band. The center of the TeV emission is determined

reflector	Davis-Cotton-design	
	focal length	4.92 m
	reflector diameter	3.40 m
	mirror segments	30 spherical glass mirrors, $\varnothing = 60$ cm, aluminized, quartz-coated
	total mirror area	$A = 8.5 \text{ m}^2$
	point spread function	$\sigma \leq 3'$
mount	alt-az (azimuthal)	
	shaft encoder	1 per axis, 1/3 resolution
	stepper motors	step width 1/3
	tracking accuracy	online: $\leq 0^\circ 1..0^\circ 3$ offline: 25''
camera	pixel	271 photomultiplier EMI 9083 KFLA
	HV supply	600..1000 V, separately adjustable for each pixel
	layout	hexag. densely packed, metallized funnels
	field of view	pixel: $0^\circ 2445$ camera: ca. $4^\circ 3$
electronics	in VME standard, mostly custom designed	
	signal digitization	120 MHz FADCs with pulse shaper ( $\tau = 12$ ns), memory $2 \times 2 \text{ k} = 34 \mu\text{s}$
	local trigger	2 neighbouring pixels within 12 ns above 8 mV (equals 6 photoelectrons)
	system trigger	2 telescopes within 70 ns, corrected for propagation delay

**Table 1.** Properties of the telescopes included in the IACT system.

by a fit of a two-dimensional Gaussian distribution to all  $\gamma$ -ray events, reconstructed in celestial coordinates. The typical angular resolution of the IACT system is  $0.1^\circ$ , but with sufficiently high event statistics the center of the TeV emission can be extracted with much better accuracy.

For a check of possible systematic errors in the telescope pointing, the HEGRA data were split up into four observing periods. For each of these observing periods, the fitted center of the TeV  $\gamma$ -rays from the Crab Nebula was compared to the position of the pulsar. Here, in the reconstruction procedure the correction for the Earth's precession was omitted. The precession changes the apparent position of any object in the sky, and is included in the pointing calibration procedure as the smallest correction which is still needed to achieve the given systematic pointing error. From the data shown in Fig. 1 one can conclude that within statistical and systematic errors, the centers of the X-ray and TeV  $\gamma$ -ray emission are well in agreement. The fitted center of TeV  $\gamma$ -ray emission follows the change in the apparent position of the source due to Earth's precession, as expected.

The window excerpts at the bottom of Fig. 1 show results from the entire data set, which was split up into three zenith angle bands. Again, the reconstructed center of the

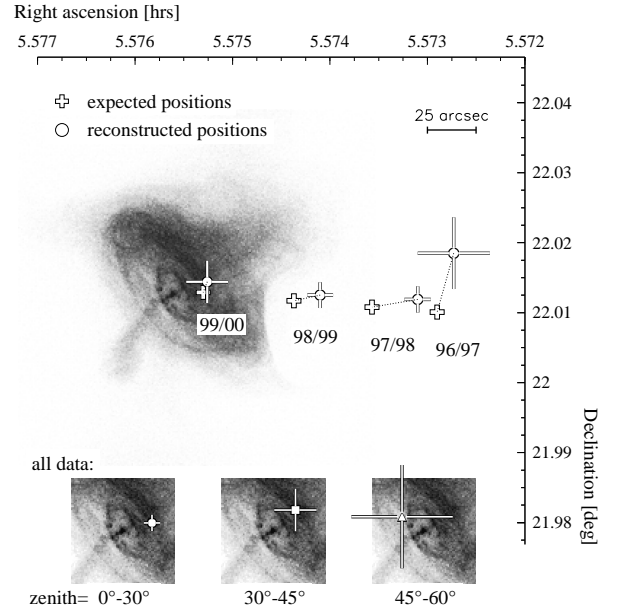


**Fig. 1.** Positions of the X-ray and TeV  $\gamma$ -ray emission from the Crab Nebula, shown in celestial coordinates. The grey-leveled image shows the recent Chandra X-ray image (courtesy of NASA/CXC/SAO). The crosses and the circles with error bars indicate the positions of the X-ray pulsar and the fitted centers of the TeV  $\gamma$ -ray emission, respectively, for four different observing seasons. The inlays at the bottom show the position of the center of the TeV emission for all data (now corrected for precession) at different zenith angle ranges.

TeV  $\gamma$ -rays corresponds well to the pulsar. Although statistics would permit, the systematic error does not allow to assign the center of TeV emission to either the pulsar or the X-ray cloud. For more details on the location and especially the extension of the Crab in TeV  $\gamma$ -rays, see Hofmann and Pühlhofer (2001) in these proceedings.

## 2.2 Point spread function

The quality of the point spread function (*psf*) of each telescope is determined by the alignment accuracy of the individual mirror tiles, which are statically attached to the reflector, and the slight deformation of the reflector itself at different elevations. The *psf* can be characterized by its on-axis width; the additional off-axis aberrations are purely of geometrical origin and therefore not susceptible to aging. The on-axis *psf* can be measured by the above mentioned *point runs*. These measurements showed that all telescopes have a *psf* with a Gaussian width of  $\sigma_{\text{psf}} = 0^\circ 03..0^\circ 04$  per axis, depending on the elevation (Pühlhofer, 2001); CT 2, which has a weaker reflector structure, shows an inferior behaviour which makes special treatment necessary.

In general, the *psf* was stable throughout the years, also with the help of mirror readjustments which were performed roughly once every year. Some problems occurred due to icing of the telescopes which temporarily lead to distortions of

the mirror tiles' alignment a few times; this could be cured by mirror readjustments. The deterioration of the *psf* was monitored as well with *point runs*, and to some extent by the background rejection power of shape cuts applied to real CR shower images; the latter method has the advantage that it can be used continuously but is less sensitive. For the analysis of a few observing periods (months) the image expectation parameters needed to be refined (e.g. Aharonian et al. (1999)), and some data were discarded.

### 3 Continuous camera electronics calibration

The monitoring and the calibration of the camera electronics is mainly covered by *laser runs* which are performed at the beginning of each observing night and occasionally repeated later on. At each telescope, nitrogen laser flashes are fed into a scintillator, which in return illuminates the camera homogeneously with a spectrum which is similar to the Cherenkov light spectrum of real showers. Each *laser run* comprises 100 laser flashes, typically at an amplitude of 80 to 100 ph.e. From the *laser runs*, the relative gains of the pixels are directly determined. The *laser runs* are used as follows:

- Every few months, the HV of all individual pixels is adjusted in order to provide a flat trigger acceptance over the camera surface; this is needed to achieve good sensitivity for the compact shower images.
- The remaining gain differences between pixels in the FADC readout are corrected offline, on the basis of the latest *laser run* result.
- The arrival time differences between pixels due to different PM transit times (few ns) is also measured. These time differences are used offline in the pulse shape analysis which converts the digitized signal shape into a pixel amplitude, the aim being noise suppression. This calibration even allowed to measure time profiles of air showers (Heß et al., 1999).

The zero offset of the FADC's (pedestals) is determined dynamically with a frequency of few seconds, from FADC memory entries which do not contain shower information.

This calibration scheme has worked robustly throughout the whole operation time of the system.

### 4 Relative sensitivity monitoring

The overall detector sensitivity needs to be monitored continuously in order to perform the energy calibration of the instrument as well as to calculate the actual collection area for  $\gamma$ -rays. Here we discuss the relative calibration with respect to the reference periods 62 ff. (summer 1997); section 5 addresses the absolute sensitivity calibration.

The sensitivity of a Cherenkov telescope is mainly given by the total mirror area, the reflectivity of the mirrors, the quantum efficiency and gain of the PMs, and finally by the trigger threshold. The optical efficiency  $\kappa_{\text{opt}}$  used here comprises the conversion of the number of Cherenkov photons to the number of photoelectrons released by the PM cathode;

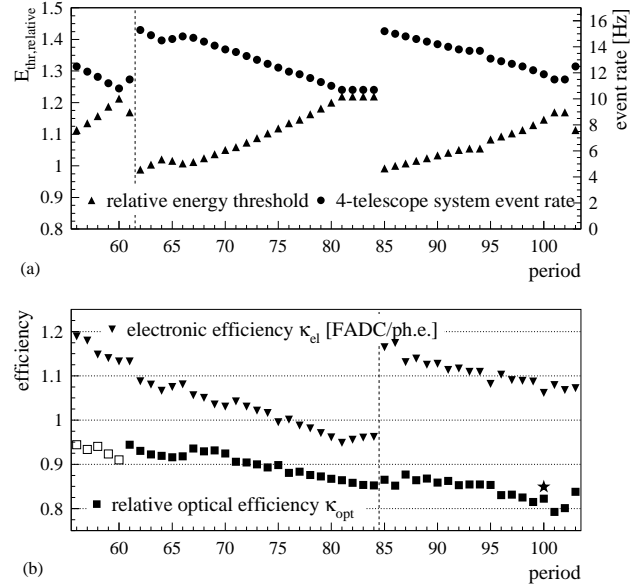


**Fig. 2.** (a) System trigger rate (converted to a 4-telescope rate) and the deduced change in the energy threshold with respect to periods 62 ff. (b) Photoelectron-to-FADC conversion factor  $\kappa_{\text{el}}$ , averaged over all telescopes, and relative optical efficiency  $\kappa_{\text{opt}}$ . The star marks the result of direct mirror reflectivity measurements. The plot ranges from January 1997 to November 2000.

$\kappa_{\text{opt}}$  is averaged over all system telescopes and is evaluated relative to some nominal value.

The PM plus electronic amplification in terms of a photoelectron-to-FADC conversion factor  $\kappa_{\text{el}}$  can be determined for each individual telescope; the method makes use of additional information obtained from the *laser runs* discussed in section 3 (Heß, 1998). These conversion factors can be measured absolutely, and were set close to one during the commissioning phase of the telescopes. The electronic efficiency  $\kappa_{\text{el}}$ , averaged over all telescopes, and  $\kappa_{\text{opt}}$  are both shown in Fig. 2b. The rise in  $\kappa_{\text{el}}$  at the position of the vertical dashed line was caused by a global increase of the HV in all cameras, which was performed to compensate for the previous gain loss.

The cosmic-ray induced event rate is a good measure for the detector threshold/sensitivity; the system practically does not trigger on noise events or local muons (Bulian et al., 1998). The trigger rate needs to be corrected for weather influences, and the actual dead time of the camera/trigger electronics must be taken into account. After these corrections, any change of the trigger event rate can be directly used to recalculate the energy threshold of the telescope system (see Fig. 2a). Since the energy threshold under optimal conditions (periods 62 ff.) was 500 GeV, we can conclude that the threshold has not exceeded 600 GeV so far.

The detector sensitivity change can be explained to a large extent with the change of  $\kappa_{\text{el}}$ . The remaining correction factor which is needed to explain the full change of the sensitivity is assigned to the optics; thereby  $\kappa_{\text{opt}}$  is determined

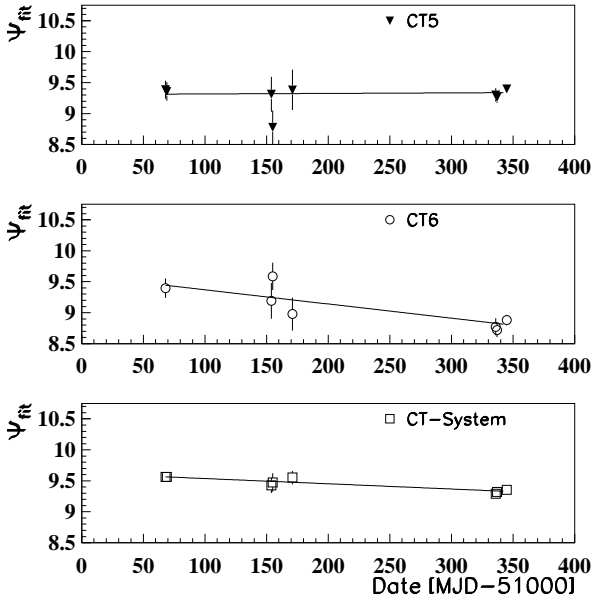


**Fig. 3.** Results of a muon run analysis, used to determine the absolute optical efficiency. The dates of the first and the last data points correspond to periods 77 and 86 in Fig. 2, respectively.

(Pühlhofer, 2001). Other values which influence the trigger rate remained unchanged: the hardware threshold of the telescope system has remained unaltered after its final adjustment to 8 mV in May 1997; also the total mirror area and the mirror alignment remained basically constant.

In summary, the aging of the HEGRA IACT system was mainly caused by a decrease of the PM gain in the camera amplification channel by roughly 6% per year; this is most probably an aging effect of the PM's last dynode. The continuous decrease of  $\kappa_{opt}$  ( $\approx 3\%$  per year) is presumably caused by a deterioration of the reflecting layer of the glass mirrors. This is also supported by direct measurements of the reflectivity of several mirrors which were performed in August 2000 (Fig. 2b, star marker at period 100).

The gradient of the time evolution of  $\kappa_{opt}$  is also confirmed by a *muon run* analysis (see section 5). For this purpose, muon rings are evaluated using pixel amplitudes which are corrected for  $\kappa_{el}$  (and hence expressed in units of ph.e.). The result (Fig. 3) is a measure of the absolute value of  $\kappa_{opt}$ .

## 5 Absolute energy threshold

To measure  $\gamma$ -ray spectra and fluxes, one needs to rely on the absolute energy calibration of the detector. Besides shower simulations and the atmospheric transmission, basically the total conversion factor between the number of Cherenkov photons and the pixel amplitude  $\kappa_{tot}$  is required for the detector simulation. The standard method is based on the comparison of the experimentally measured trigger rate induced by charged CRs with the predicted rate derived from detailed Monte Carlo simulations (Konopelko et al., 1999). Due to

uncertainties in the CR flux, spectrum and composition, this method has an uncertainty of  $\approx 15\%$  in the energy estimate.

Two alternative methods to obtain  $\kappa_{tot}$  were investigated:

- *Muon runs*: When a muon hits the telescope reflector, the total number of Cherenkov photons hitting the mirror depends only on event characteristics, which can be determined from geometrical properties of the measured muon ring image. For such runs, only special trigger conditions (no system trigger, 5 pixels above 6 mV) are required.

- *Laser illumination using a calibrated photodiode as reference*: This method requires a stabilized laser and was only temporarily installed. The laser illuminates the whole reflector; a filter is needed to attenuate the laser light from the intensity level accessible to the photodiode down to the level where the PM camera is sensitive (e.g. Fraß et al. (1997)).

Both methods have the potential to reduce the error on the energy scale down to a few percent. However, systematic effects still limit the evaluation of the parameters. Hence, we currently quote an uncertainty of 15% as a conservative estimate.

## 6 Conclusion

Throughout the years, the HEGRA IACT system performance has been well monitored and found to be stable. The experience gained with HEGRA will be profitable for future projects like the H.E.S.S. telescope system which is currently under construction in Namibia.

*Acknowledgements.* The support of the German ministry for Research and technology BMBF and of the Spanish Research Council CICYT is gratefully acknowledged. We thank the Instituto de Astrofísica de Canarias for the use of the site and for supplying excellent working conditions at La Palma. We gratefully acknowledge the technical support staff of the Heidelberg, Kiel, Munich, and Yerevan Institutes.

## References

- Aharonian, F. A., Akhperjanian, A. G., Barrio, J. A. et al., *A&A* 342, 69–86, 1999.
- Bulian, N., Daum, A., Hermann, G. et al., *Astropart. Phys.* 8, 223–233, 1998.
- Daum, A., Hermann, G., Heß, M. et al., *Astropart. Phys.* 8, 1–11, 1997.
- Fraß, A. et al., *Astropart. Phys.* 8, 91–99, 1997.
- Heß, M., PhD thesis, Ruprecht-Karls-Universität Heidelberg, Heidelberg, Germany, 1998.
- Heß, M., Bernlöhr, K., Daum, A. et al., *Astropart. Phys.* 11, 363–377, 1999.
- Hofmann, W. and Pühlhofer, G., The size of the emission region of VHE gamma rays in the Crab Nebula, these proceedings, 2001
- Konopelko, A., Hemberger, M., Aharonian, F. et al., *Astropart. Phys.* 10, 275 ff., 1999.
- Pühlhofer, G., Daum, A., Hermann, G., et al., *Astropart. Phys.* 8, 101–108, 1997.
- Pühlhofer, G., Phd Thesis, Ruprecht-Karls-Universität Heidelberg, Heidelberg, Germany, 2001.